

Multifunctional Materials

Exploiting Molecular Self-Assembly: From Urea-Based Organocatalysts to Multifunctional Supramolecular Gels

Eva-Maria Schön,^[a] Eugenia Marqués-López,^[b] Raquel P. Herrera,^{*[b]} Carlos Alemán,^[c] and David Díaz Díaz^{*[a, d]}

Abstract: We describe the self-assembly properties of chiral *N,N'*-disubstituted urea-based organocatalyst **1** that leads to the formation of hierarchical supramolecular gels in organic solvents at low concentrations. The major driving forces for the gelation are hydrogen bonding and π - π interactions according to FTIR and ¹H NMR spectroscopy, as well as quantum-mechanical studies. The gelation scope could be interpreted based on Kamlet-Taft solvatochromic parameters. TEM, SEM, and AFM imaging revealed that a variety of morphologies including helical, laths, porous, and lamellar nanostructures could be obtained by varying the solvent. Experimental gelation tests and computational structural analysis of various structurally related compounds proved the exist-

tence of a unique set of molecular interactions and an optimal hydrophilic/hydrophobic balance in **1** that drive the formation of stable gels. Responses to thermal, mechanical, optical, and chemical stimuli, as well as multifunctionality were demonstrated in some model gel materials. Specifically, **1** could be used for the phase-selective gelation of organic solvent/water mixtures. The gel prepared in glycerol was found to be thixotropic and provided a sensitive colorimetric method for the detection of Ag^I ions at millimolar concentrations in aqueous solution. Moreover, the gel matrix obtained in toluene served as a nanoreactor for the Friedel-Crafts alkylation of 1*H*-indole with *trans*- β -nitrostyrene.

Introduction

Multifunctional stimuli-responsive structures have drawn great attention in the last decade due to their potential use in advanced devices and help to expand fundamental scientific understanding.^[1] Such systems possess properties that allow them to perform more than one function in a device or material in which interfacial properties are coupled. Inspired by abundant examples in nature for which multifunctionality is a norm (e.g., multifunctional extracellular matrices), the main need for the development of multifunctional materials is that specific problems cannot always be solved by the mere combination

of materials with different functions due to critical technological barriers.

In the above context, self-assembled gels^[2] constitute promising candidates to achieve multifunctional materials for different applications.^[3] In contrast to chemical gels,^[4] which are based on covalent bonds, physical or supramolecular gels^[5] are made of either low-molecular-weight (LMW) compounds or polymers through noncovalent interactions (e.g., hydrogen bonding, π - π stacking) that usually provide a reversible response to external stimuli (e.g., gel-to-sol thermal transition). In general, the solidlike appearance of gels is derived from a very efficient entrapment of the solvent molecules, usually by capillary forces,^[6] into the interstices of a solid matrix with high surface area formed upon the entanglement of 1D supramolecular fibrillar assemblies. There is an extensive collection of functional moieties that can induce the formation of such assemblies in solution.^[2c,3c,5] Among those, the ureide group is one of the best-known hydrogen-bonding functional groups, which has been widely used to fabricate valuable supramolecular architectures,^[7] including gel networks based on mono- or polyurea gelators,^[8] by a directional assembly process.

Herein, we report and rationalize the self-assembly properties of a known urea-based organocatalyst that leads to the formation of multifunctional and multiresponsive supramolecular gels in organic solvents.

[a] Dr. E.-M. Schön, Prof. D. D. Díaz

Institut für Organische Chemie, Universität Regensburg
Universitätsstr. 31, 93053 Regensburg (Germany)
E-mail: David.Diaz@chemie.uni-regensburg.de

[b] Dr. E. Marqués-López, Dr. R. P. Herrera

Departamento de Química Orgánica,
Instituto de Síntesis Química y Catálisis Homogénea (ISQCH)
CSIC-Universidad de Zaragoza
Pedro Cerbuna 12, 50009 Zaragoza (Spain)
E-mail: raquelph@unizar.es

[c] Prof. C. Alemán

Departament d'Enginyeria Química
- ETSEIB and Center for Research in Nano-Engineering
Universitat Politècnica de Catalunya, Av. Diagonal 647
08028 Barcelona (Spain)

[d] Prof. D. D. Díaz

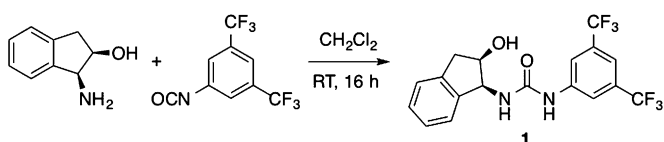
IQAC-CSIC, Jordi Girona 18-26, 08034 Barcelona (Spain)

Supporting information for this article is available on the WWW under
<http://dx.doi.org/10.1002/chem.201402436>.

Results and Discussion

Design and synthesis of compounds

During our research programs focused on both the development of new organocatalysts and the use of unconventional reaction media (e.g., softgel materials, ionic liquids), we paid close attention to the tendency of the known *N,N'*-disubstituted urea-based organocatalyst (+)-**1**^[9] (Scheme 1) to increase the viscosity of some common organic solvents leading to the in situ formation of jelly-like lumps during its synthesis. We decided to investigate in detail the gelation ability of **1** after taking into consideration the facile and scalable synthesis of this type of compound, its intrinsic potential as a multifunctional molecule, and the previous studies reported so far on urea-based organogelators.^[8] Compound **1** is easily accessible by an equimolar reaction of commercial (1*S*,2*R*)-1-amino-2,3-dihydro-1*H*-inden-2-ol and 3,5-bis(trifluoromethyl)phenyl isocyanate in methylene chloride at room temperature (Scheme 1).



Scheme 1. Synthesis of the *N,N'*-disubstituted urea (+)-**1**.

To correlate the structural features of **1** with the gelation properties, we designed and synthesized a library of analogous compounds **2–7** (Figure 1) following a similar synthetic procedure. The structural complexity of **1** was greatly reduced by replacing both aromatic residues by 3,5-bis(trifluoromethyl)phenyl groups (compound **3**) or phenyl groups (compound **4**). To study the influence of the stereochemical configuration of the stereogenic centers we also carried out the synthesis of the diastereomer **5**. The evident intramolecular hydrogen bonding between the carbonyl group and the hydroxyl group at the 2,3-dihydro-1*H*-indene residue inspired us to prepare compound **6** lacking the hydroxy group and thiourea derivative **2**. Additionally, we considered the removal of only the bulky tri-

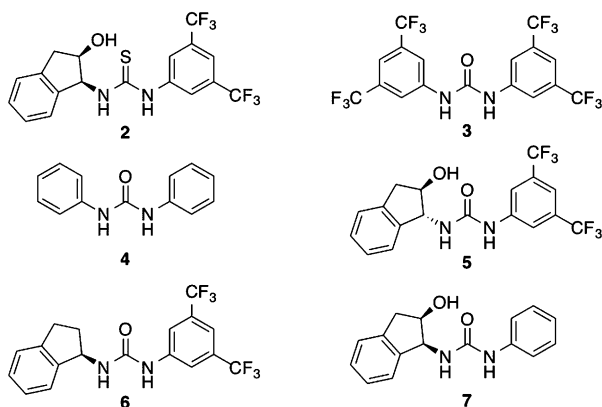


Figure 1. Library of additional compounds **2–7** used in this work.

fluoromethyl groups (compound **7**) since they are also known to lower the basicity and/or confer distinctive solvation properties of organic compounds, which play a key role on the gelation phenomena.^[2–6]

All synthesized compounds were satisfactorily characterized after purification by silica gel column chromatography.^[10]

Gelation ability and gel stability

The gelation ability of urea **1** was first evaluated for 33 different solvents by using the classical heating-cooling process within a broad concentration range. The state of the resulting mixture was initially examined by the “stable-to-inversion of a test tube” method. After the visual inspection, the viscoelastic gel nature of those samples showing no gravitational flow upon turning the vial upside-down was further confirmed by oscillatory rheological measurements in model solvents (vide infra).

We were delighted to observe that compound **1** induced gelation of 14 solvents at a critical gelation concentration (CGC) between 3 and 50 g L⁻¹ (Table 1) (the procedure to determine the CGC is described in the Experimental Section). These values imply the immobilization of 10²–10³ (order of

Table 1. Gelation scope of **1**, optical appearance (OA) of the gels, critical gelation concentrations (CGC), gelation times, and gel-to-sol transition temperatures (T_{gel}).^[a]

Entry	Solvent	Phase	OA	CGC [g L ⁻¹]	Gelatin time	T_{gel} ^[d] [°C]
1	toluene	G	T	3	30 ± 5 min	55
2	benzene	G	T	3	30 ± 5 min	41
3	chlorobenzene	G	T	3.6	7 ± 2 min	54
4	1,2-dichlorobenzene	G	T	3.6	7 ± 2 min	62
5	1,3-dichlorobenzene	G	T	3.6	7 ± 2 min	64
6	mesitylene	G	T	3.5	5 ± 1 h	nd
7	<i>o</i> -xylene	G	T	3.5	8 ± 2 h	nd
8	<i>m</i> -xylene	G	T	3.5	5 ± 1 h	nd
9	nitrobenzene	G	O	50	30 ± 5 min	41
10	glycerol ^[b]	G ^[c]	T	3	40 ± 10 min	74
11	methylene chloride	G	T	4	20 ± 5 min	46
12	chloroform	G	T	7	45 ± 10 min	nd
13	carbon tetrachloride	G	T	5	10 ± 5 min	84
14	nitromethane	G ^[c]	T	25	24 h	nd

[a] Gels obtained after heating-cooling cycle. Volume = 1 mL. Abbreviations: G = gel; T = transparent gel; O = opaque gel; nd = not determined due to gel weakness. [b] Commercial sample contained 10 wt.% water. [c] A minor fraction of insoluble material remained. [d] Values calculated at the CGC by the inverse flow method. Estimated error ± 2 °C.

magnitude) solvent molecules per gelator molecule. In most cases, complete gelation was achieved within 5 min and 1 h. A clear preference for gelation of aromatic (entries 1–9) and chlorinated solvents (entries 11–13) was observed. All organogels obtained at the CGC were transparent except in nitrobenzene, which was completely yellowish opaque, which indicated the formation of aggregates smaller than the visible wavelength range ($\lambda = 400\text{--}700\text{ nm}$) (Figure 2). Such optical differences highlight the importance of the interactions between sol-

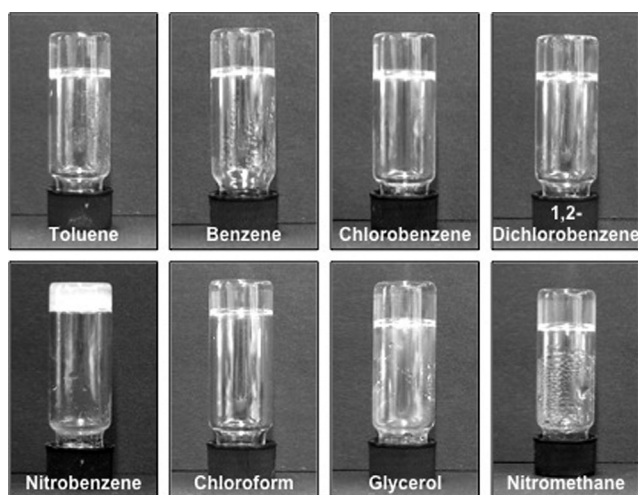


Figure 2. Representative digital photographs of upside-down vials containing organogels made of **1** in different solvents at the CGC as shown in Table 1.

vent and gelator molecules for the growth and stabilization of the supramolecular network.

Compound **1** was found to be insoluble in both water and *n*-heptane upon heating and/or extensive sonication (2 h), whereas stable clear solutions were obtained at 50 g L⁻¹ upon heating-cooling in acetonitrile, ethyl acetate, ethanol, methanol, DMSO, DMF, dimethylacetamide, THF, diethyl ether, 1,2-dimethoxyethane, acetone, cyclohexanone, 3-methyl-butan-2-one, methyl *tert*-butyl ether, 1,4-dioxane, benzonitrile, and rapeseed oil. Exceptionally, gels in nitromethane (Table 1, entry 14) and 90 wt.% glycerol (entry 10) could also be obtained. The case of glycerol is particularly interesting since 1) it was the only alcoholic solvent in which gelation was successful and 2) it is a nontoxic, nonhazardous, nonvolatile, and biodegradable solvent widely used in manifold industries including, among others, food, antifreeze, pharmaceutical, and personal care applications.^[11]

Based on the solvent parameters (*vide infra*) and to optimize the number of experiments, we chose three representative model solvents (i.e., CH₂Cl₂, toluene, and glycerol), among those gelled by **1**, to conduct comparative gelation experiments with the structurally related compounds **2–7**. Very interestingly, the analogues **2–6** did not show any gelation ability in the model solvents. Only compound **7**, lacking the trifluoromethyl groups, was able to form a transient weak gel in toluene at a concentration of 3 g L⁻¹, and a stable gel in glycerol at 5 g L⁻¹. Compound **7** required not only a five-fold higher concentration than **1** to form a steady homogeneous gel in glycerol, but also an approximately five-fold longer gelation time. These results clearly suggested the existence of unique inter- and/or intramolecular interactions as well as an optimum balance between hydrophobic and hydrophilic domains that largely favor the spontaneous self-assembly of **1** in solution leading to supramolecular aggregates with a lifetime long enough to allow their anisotropic growth and consequent stable gel formation.

It is worth mentioning that all our attempts to obtain isotropic solutions of potential gelators in the model solvents and subsequent formation of stable gels using either 1) sonication instead of the heating-cooling cycle or 2) predissolving the compound in the minimum amount of a nonprotic polar solvent, such as DMSO followed by addition of the testing solvent (e.g., maintaining the CGC value as given in Table 1) at room temperature were fruitless.

Thermal and temporal stability

The organogels were found to be thermoreversible and stable to multiple heating-cooling cycles without any detriment on the gelation ability and gel properties. The gel-to-sol transition temperatures (T_{gel}) of all organogels were determined by the inverse flow method.^[12] As this method depends on the cooling rate and thermal history, among other factors, the values were correlated for model examples with the first endothermic transition observed by differential scanning calorimetry (DSC) (see Figure S5 in the Supporting Information). Consistently with the formation of more entwined networks, T_{gel} increased considerably until reaching a plateau with increasing the concentration of the urea gelator **1** (e.g., ΔT_{gel} (toluene) $\sim 38^\circ\text{C}$ upon increasing 2.3-fold the concentration defined by the CGC, Figure 3). Interestingly, we found that the amount of

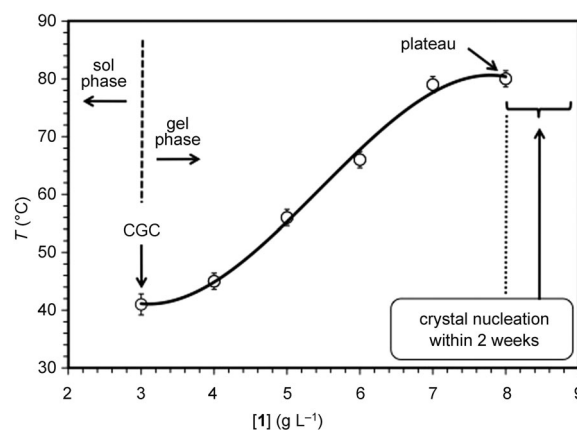


Figure 3. Phase diagram and evolution of T_{gel} as a function of the concentration of gelator **1** in toluene.

water present in commercial 90 wt.% glycerol was necessary to prepare the isotropic solution of the gelator and subsequent gels. Attempts to dissolve **1** in 99 wt.% glycerol upon heating were unsuccessful. The T_{gel} values increased considerably from 60 to 90 wt.% glycerol (e.g., 64°C at 70 wt.% and 74°C at 90 wt.%). The gels prepared with 60 wt.% glycerol were too fragile to resist inversion of the vial.

Organogels made of **1** at the CGC remained stable for at least one month when stored undisturbed at room temperature. After this period, optical microscopic imaging of some materials revealed a very slow crystal growth (Figure 4), which clearly underlines the thermodynamic equilibrium between gel and crystalline phases.^[13] Nevertheless, the robustness of the

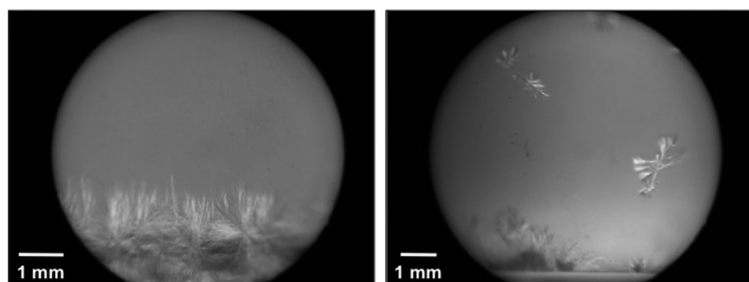


Figure 4. Optical microscope picture showing crystal formation in the gel matrix made of **1** at CGC (left) and at 15 g L^{-1} (right) after five weeks.

gel network permitted its coexistence with the crystal nucleation for several months while remaining stable to the inversion of the vial. As expected, the crystallization kinetics also increased with gelator concentration.

Influence of enantiomeric purity

As chirality plays a key role in the formation of gels,^[14] we investigated the gelation ability of **1** prepared at different enantiomeric excesses by mixing appropriate amounts of the pure enantiomers (+)-**1** and (–)-**1**. Stable gels upon inversion of the vials were only obtained when the enantiomerically pure urea gelator was used (Figure 5 and Figure S14 in the Supporting

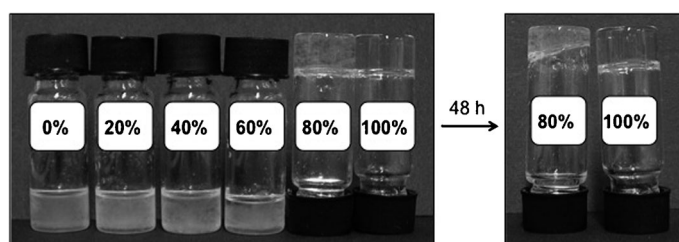


Figure 5. Influence of enantiomeric purity on the gelation ability of **1**. Percent values indicate the enantiomeric excess of **1** used in each case.

Information). As expected, (+)-**1** and (–)-**1** showed identical gelation properties. Precipitation or small pieces of jelly-like aggregates were observed when the urea compound was used with enantiomeric excesses below 80%. The material made from the urea with 80% ee consisted of a mixture of precipitate and gel (gelation time in this case was double than when using pure **1**) and could support the inversion of the vial. However, after 48 h, the material collapsed and only the sample made with 100% ee remained homogeneous, transparent, and stable to the inversion of the vial.

Phase-selective gelation ability

Selective organogelation from organic solvent/water mixtures is an important task in environmental remediation.^[15] This ability has been reported for some efficient LMW organogelators,^[15,16] albeit it is still an uncommon feature in the area of supramolecular gels. Interestingly, water-insoluble urea **1** also

showed this ability with a broad scope of organic solvents. Typically, a 1:1 v/v mixture containing water and any water-immiscible organic solvent from Table 1 was heated and vigorously shaken in the presence of **1** at the corresponding CGC. After cooling down the homogeneous dispersion to room temperature, the organic phase was entirely gelled, whereas the water phase remained liquid. Depending on the density of the organic phase, the gel material was located either above or below the water layer. For the latter case, the gel was stiff enough to hold the upper water phase upon inversion of the vial (Figure 6A). Both phases could be further separated by simple decantation or filtration. The thermal stability of the gel phase remained very similar to the gel obtained from the pure organic solvent (i.e., ΔT_{gel} ca. $\pm 5^\circ\text{C}$).

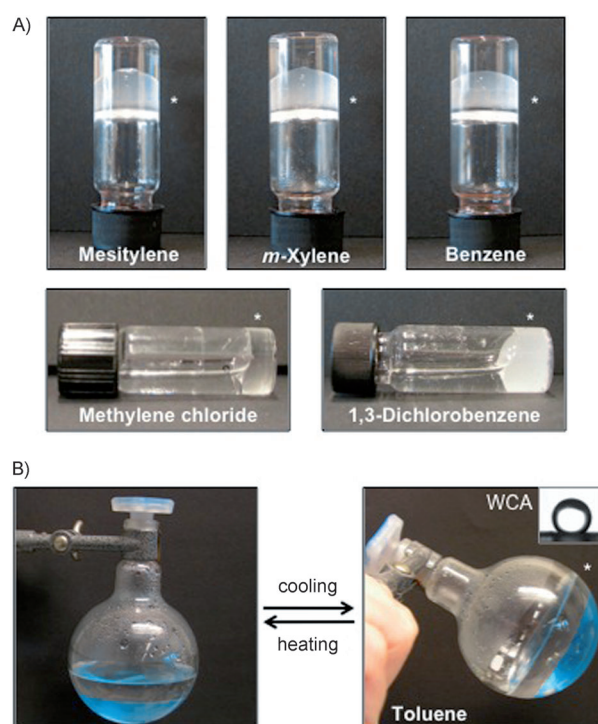


Figure 6. A) Representative digital photographs of phase-selective gelation of organic solvent/water mixtures (total volume = 2 mL). The organic solvent is marked with an asterisk. B) High-scale phase-selective gelation of 1:1 v/v toluene/water mixture (total volume = 0.1 L^{-1}). Water-soluble T-1824 dye (Evans Blue) was used to differentiate better both phases. The aqueous phase remained completely liquid after gelation of the upper organic phase as evidenced by usual spinning of the magnetic stir bar. Inset in the bottom-right picture) Photograph of a water drop on a thin film of the gel made in toluene.

Moreover, the phase-selective gelation could be scaled up 50-fold without any difficulty (Figure 6B). When the aqueous phase was stained with Evans Blue, the organic phase remained clear upon gelation, which indicated no diffusion of water through the interface. This is also understandable if we consider the intrinsic hydrophobicity of polyfluorinated **1** (e.g., water contact angle (WCA) $\sim 110^\circ$), which is even enhanced

upon the formation of the nanostructured gel network as a result of combining the low surface energy with a superior roughness (e.g., WCA of the xerogel obtained from the gel made in toluene $\sim 140^\circ$).^[17] Moreover, we observed that the model gels remained stable in the presence of water, NaOH (0.1 M), or even HCl (0.1 M) aqueous solutions (the experiments were carried out by placing 1 mL of the test solution on top of 1 mL of gel material).

Correlation between gelation ability and solvent parameters

To rationalize the organogel formation we built and compared 3D plots according to the Kamlet–Taft solvatochromic parameters (i.e., hydrogen-bond donor ability (α), hydrogen-bond acceptor (β), and polarizability (π^*))^[18] and the Hansen solubility parameters (i.e., dispersive interactions (δ_d), dipolar interactions (δ_p), and hydrogen bonding (δ_h) interactions) (see Table S1 in the Supporting Information).^[19] The Kamlet–Taft solvent parameters have been associated with the ability of forming hydrogen-bonded gels (α value), thermal stability of the networks (β value) and stabilization of charges and dipoles during the gelation process (π^* value).^[20] With glycerol being the only exception, these parameters clearly delimited a gelation cuboid space (ca. 0.045 cubic units) defined by the following approximate dimensions: $0 < \beta < 0.3, 0 < \alpha < 0.2$ and $0.25 < \pi^* < 1$ (Figure 7). These limits indicate that π^* has the lower influence in the formation of gels, whereas having relatively low and balanced hydrogen-bond donor and acceptor abilities is critical. On the other hand, Hansen solubility parameters also provided an acceptable gelation space albeit only approximately 70% of the gelled solvents were found inside the cuboid space defined approximately by $0 < \delta_p < 9, 17.5 < \delta_d < 20$ and $0.5 < \delta_h < 6$ (see Figure S3 in the Supporting Information). Thus, dipolar interactions seem to be the most critical

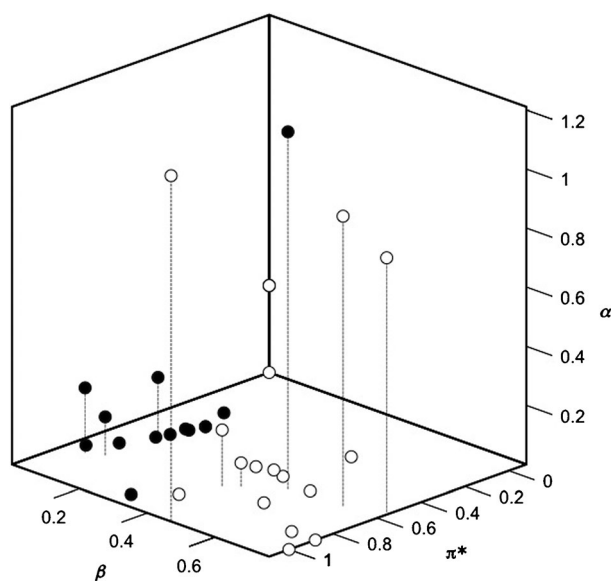


Figure 7. 3D scattering plot showing the results of the gelation tests and the Kamlet–Taft parameters of each solvent. ● = gelled solvents; ○ = non-gelled solvents.

ones for a Hansen model, although a model based on the Kamlet–Taft parameters is comparatively more adequate for developing a gelation model in our case. No significant tendencies were observed for the gel properties (i.e., CGC, T_{gel}) in function of the individual solvent parameters.

Driving force study and computer modeling

FTIR measurements

In agreement with other urea-based gelators, comparison of the FTIR spectra of model xerogels prepared from the corresponding organogels by freeze-drying with those in solution phase and **1** in the solid state supported the involvement of hydrogen bonding in the gelation phenomenon (see Figure S4 in the Supporting Information). In general, the gel-based materials displayed $-\text{NH}$ stretch vibration bands at approximately $3311\text{--}3257\text{ cm}^{-1}$, whereas amide I ($\text{C}=\text{O}$) and amide II vibrations appeared at approximately $1641\text{--}1637$ and $1562\text{--}1546\text{ cm}^{-1}$, which typically correspond to molecules aggregated by hydrogen bonding (non-hydrogen-bonded amides display the above vibrations at approximately 3430 , 1660 , and 1515 cm^{-1} , respectively). No vibrational bands were observed in the region of $3700\text{--}3500\text{ cm}^{-1}$ ($-\text{OH}$ stretching, free), which suggests that the hydroxyl group is also hydrogen bonded, likely to the carbonyl group in an intramolecular manner. Interestingly, the solid and freshly prepared **1** showed the selected absorption bands at the same positions within the experimental uncertainty ($\pm 2\text{ cm}^{-1}$), which indicates that urea **1** is also aggregated by hydrogen bonding in the solid state and hence the existence of some similarity between the solid and the gel structures. In agreement, although compound **1** has a very low degree of crystallinity as deduced from its PXRD pattern, the xerogel obtained by freeze-drying the corresponding organogel in toluene still preserved part of this crystallinity (i.e., major broad peak centered at 20° , $2(\theta)$) (Figures S16–17).

Temperature-dependent ^1H NMR spectroscopic experiments

As we have observed with peptide-based physical gels,^[21] the protons involved in the stabilization of the supramolecular network could be experimentally tracked by NMR spectroscopic experiments at different temperatures. Thus, we recorded ^1H NMR spectra of the model organogel made of **1** in $[\text{D}_8]\text{toluene}$ within a temperature range for which both gel and solution phases could be gradually interconverted. An upfield shift (i.e., $\Delta\delta/\Delta T \approx 5.3 \times 10^{-5}\text{ ppm K}^{-1}$) of the $-\text{NH}$ urea protons was first observed in the range of $27\text{--}35^\circ\text{C}$, followed by a clear downfield shift (i.e., $\Delta\delta/\Delta T \approx 1.5 \times 10^{-4}\text{ ppm K}^{-1}$) in the range of $35\text{--}55^\circ\text{C}$ (gel phase). A further increase of the temperature until 70°C (solution phase) was accompanied by another upfield shift (i.e., $\Delta\delta/\Delta T \approx 6.3 \times 10^{-3}\text{ ppm K}^{-1}$) (Figure 8).

The unusual and diffident upfield shift observed at the beginning of the experiment is presumably associated with a homogenization process of the sample. The marked maximum point observed at 55°C ($\sim 328\text{ K}$; breaking of hydrogen bonding) matched with the T_{gel} of the material. The $-\text{OH}$ proton displayed a very similar chemical shift pattern. All other protons

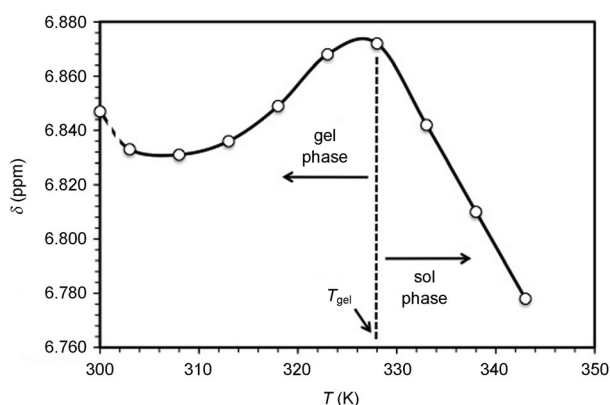


Figure 8. Representative temperature-induced chemical shifts of the $-NH$ urea proton of **1** in $[D_6]$ toluene.

not involved in hydrogen bonding showed the opposite pattern (i.e., upfield shift until 55°C and subsequent downfield shift until 70°C) (see Figure S6 in the Supporting Information). Overall, these results are in good agreement with the marked influence of hydrogen bonding and π - π stacking interactions in the gelation process, involving a different type of disassembly process during the initial heating period.^[22]

It should be noted that the ^1H NMR spectroscopic signals of gelator molecules that form the gel network are unlikely to be observed due to long correlation times.^[23] The observed signals are then attributed to small amounts of gelator molecules, either aggregated or disaggregated, dissolved in the immobilized solvent. Thus, the improvement of the signals resolution and increment of their intensity upon heating (see Figure S6 in the Supporting Information) is associated with the enhancement of molecular mobility and segregation of the network.

Quantum-mechanical calculations

To evaluate the strength of the intermolecular interactions in **1**-**7**, quantum-mechanical calculations at the M06L/6-31+G(d,p) level were performed on model complexes formed by two interacting molecules (dimers). More specifically, seven different complexes were constructed for the dimer of **1** by considering stabilizing π - π stacking, dispersion, hydrogen bonding, and dipole-dipole intermolecular interactions. After this, the seven dimers of **1** were used to construct equivalent dimers for **2**-**7** (i.e. introducing the required changes in the chemical structure without altering the relative orientation between the cores of the two molecules). All these structures were used as starting points for complete geometry optimizations in dichloromethane solution.

Figure 9, which represents the interaction energies calculated in absence of external forces (ΔE_i^{gp}) and in CH_2Cl_2 solution (ΔE_i^{sol}), indicates that the association is significantly more favored for **1** than for the compounds **2**-**7**, which is fully consistent with the gelation abilities discussed above. Although the interaction energy increases with the polarity of the environment, the functionality and molecular architecture of **1** is the most appropriate for the formation of intermolecular interactions. Figure 10A, which depicts the dimer of **1** with lowest

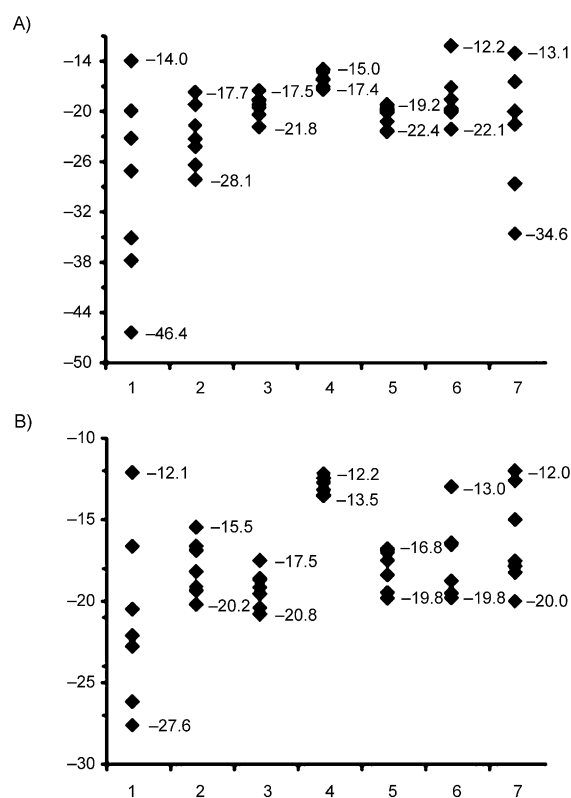


Figure 9. Range of variation of A) ΔE_i^{gp} and B) ΔE_i^{sol} (both in kcal mol^{-1}) for the calculated dimers of compounds **1**-**7**.

ΔE_i^{gp} and ΔE_i^{sol} (-46.4 and $-27.6 \text{ kcal mol}^{-1}$, respectively) reveals the coexistence of one parallel π - π stacking interaction, three hydrogen-bond interactions (two $\text{N-H}\cdots\text{O}$ and one $\text{O-H}\cdots\text{O}$), and one $\text{C-H}\cdots\pi$ stabilizing interaction. In addition, dis-

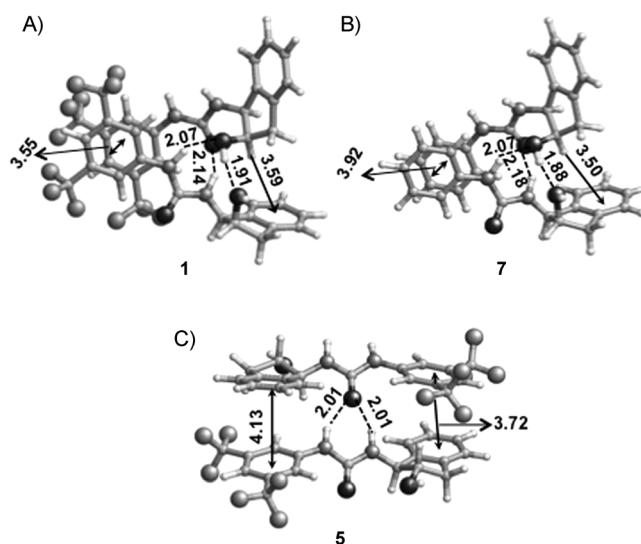


Figure 10. Representation of the most stable complex calculated for dimers of a) **1**, b) **7**, and c) **5**. Intermolecular hydrogen bonds (---), π - π stacking (\leftrightarrow) and $\text{C-H}\cdots\pi$ interactions (\rightarrow) are displayed. Labels refer to the distances (in \AA) found for each stabilizing interaction: $\text{H}\cdots\text{O}$ distance in hydrogen bonds; center of masses to center of masses in π - π stacking; and $\text{H}\cdots$ center of masses in $\text{C-H}\cdots\pi$. See the Supporting Information for a color version of this figure.

tances displayed in Figure 10A are typically associated with strong secondary interactions. Interestingly, the dimer of **7** with lowest ΔE_i^{gp} and ΔE_i^{sol} (-34.6 and -20.0 kcal mol $^{-1}$, respectively), which is depicted in Figure 10B, shows the same number and type of interactions. As the only difference between **1** and **7** refers to the $-CF_3$ groups, which have been eliminated in the latter, the reduction in the interaction energies that amounts to approximately 25% should be attributed to the fluorine-induced electrostatic and dispersive interactions.^[24]

Both the number and, especially, the strength of intermolecular interactions are lower for dimers of compounds **2–4**, as is evidenced in the complex of lowest ΔE_i^{gp} and ΔE_i^{sol} displayed for each compound in Figure S21 (Supporting Information). This reduction is essentially due to the thiourea in **2**, which forms weaker hydrogen bonds than the replaced urea, and to the removal of the hydroxyl group in **3** and **4**, which affects not only intermolecular interactions but also to the interaction of the dimers with the solvent. Thus, the dimerization of **2** results in the formation of two weak N–H...S hydrogen bonds and two parallel π – π stacking interactions (Figure S21A, Supporting Information), whereas the most stable dimer of **3** and **4** shows two N–H...O hydrogen bonds and two π – π stacking interactions, one with the aromatic rings arranged in parallel and the other with a T-shaped disposition (Figure S21B and S21C, Supporting Information). Compound **5** deserves special attention since its chemical composition is identical to that of **1**, the only difference between the two species involving the stereochemistry of the urea group with respect to the five-membered ring. As it can be seen in Figure 10C, which displays the dimer of **5** with lowest ΔE_i^{gp} and ΔE_i^{sol} (-22.4 and -20.1 kcal mol $^{-1}$, respectively), the hydroxyl groups only interact with the solvent, the stereochemistry precluding their participation in stabilizing intermolecular hydrogen bonds. Consequently, the interval of variation of ΔE_i^{gp} and ΔE_i^{sol} is significantly lower for **5** than for **1**. Indeed, comparison of the energies computed for the dimers of the stereoisomers displayed in Figure 10A and 10C indicates that **5** is less stable than **1** by 8.3 and 11.8 in dichloromethane solution and in the gas-phase, respectively. The most stable dimers of compound **6** in terms of ΔE_i^{gp} and ΔE_i^{sol} are different (Figures S21D and S21E, Supporting Information, respectively), even though the characteristics of the secondary interactions found for these complexes are very similar to those described above for **2–5**.

Morphological characterization of organogels

The fibrillar nature of the gel networks was evidenced by TEM imaging of the corresponding xerogels. Typically, entangled supramolecular fibers with average diameters in the range of 10–30 nm and a few micrometer lengths were observed for different solvents (Figure 11). Complementary images of dense fibrillar bundles with average heights between 15 and 30 nm were also obtained by AFM. Interestingly, a close look to the photographs revealed that the fibers corresponding to the gel in some solvents like toluene displayed a helical morphology (Figure 11 and Figure S11 in the Supporting Information).

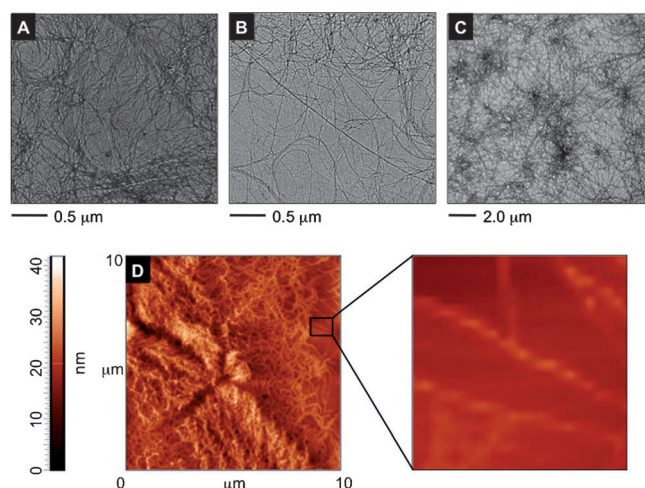


Figure 11. Representative TEM and AFM images of xerogels obtained from the corresponding organogels prepared at the CGC as shown in Table 1. The high aspect ratio of the images suggests a highly anisotropic supramolecular assembly. TEM: A,B) toluene, C) methylene chloride. AFM: D) Benzene.

SEM imaging of the xerogels revealed a remarkable influence of the solvent nature on the morphology of the supramolecular aggregates (Figure 12 and Figure S10 in the Supporting Information). For instance, accurate laths of 100–400 nm widths were obtained with mesitylene (1,3,5-trimethylbenzene), whereas dense ribbonlike fibrillar structures ($\varnothing \sim 10$ –40 nm) were observed in toluene, benzene, and xylenes. In sharp contrast, chlorinated solvents provided fibrillar and highly interconnected macroporous structures ($\varnothing \sim 100$ –500 nm). Other solvents, such as nitromethane featured unique lamellar layer microstructures that were not observed with other solvents. The exact mechanism for which each solvent induced a specific morphology remains elusive.

Moreover, the anisotropic and thermoreversible nature of the organogels enabled us to turn on/off their birefringence under polarized light (Figure 13 and Figure S12 in the Supporting Information), an important property widely searched for in optical devices.^[25]

Oscillatory rheological measurements

Dynamic rheological measurements of some model materials confirmed their viscoelastic properties. Typically, the storage modulus G' and loss modulus G'' were first measured at room temperature as a function of the frequency (dynamic frequency sweep experiment, DFS) and shear strain (dynamic strain sweep experiment, DSS) to establish the linear viscoelastic regime (Figure 14 and Figures S7–S9 in the Supporting Information). A relatively constant $\tan \delta$ (G''/G') value during the DFS measurement was indicative of a good tolerance of the gel against external forces. Within the linearity limits of deformation (e.g., 1 Hz frequency and 0.1% strain), G' was found always one order of magnitude higher than G'' (e.g., $G' \approx 2.3 \times 10^4$ Pa, $G'' \approx 6.8 \times 10^3$ Pa, for the gel made of **1** in toluene at 5 g L $^{-1}$). The stability of the material over time at room temper-

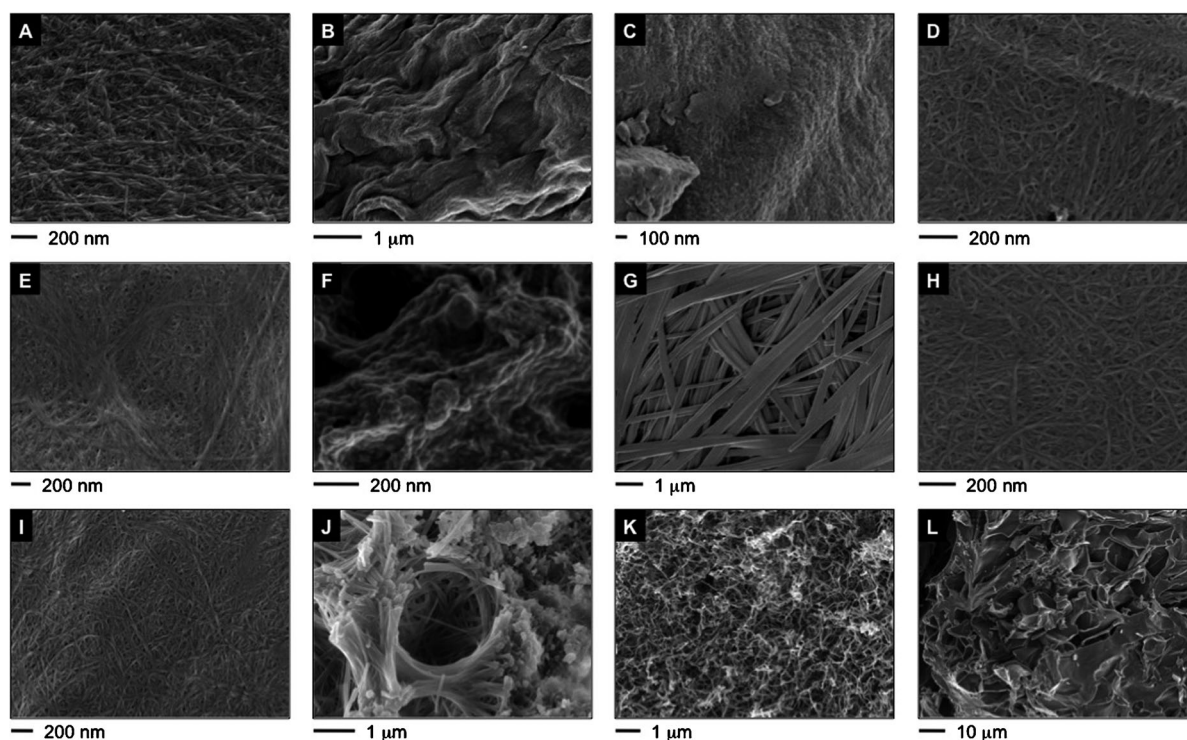


Figure 12. Representative SEM images of xerogels obtained by freeze-drying the corresponding organogels prepared in different solvents at the CGC as shown in Table 1. A) benzene, B) toluene, C) chlorobenzene, D) 1,3-dichlorobenzene, E) 1,2-dichlorobenzene, F) nitrobenzene, G) mesitylene, H) *m*-xylene, I) *o*-xylene, J) methylene chloride, K) carbon tetrachloride, L) nitromethane.

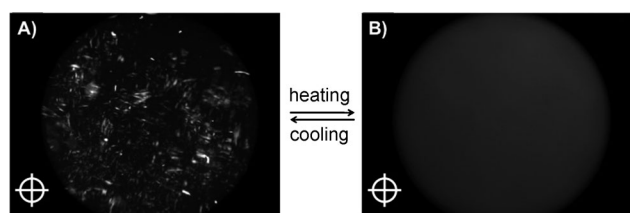


Figure 13. Polarized light microscope images of A) organogel made of 1 in methylene chloride at CGC and B) the corresponding solution obtained upon the thermal gel-to-sol transition. The polarizing filter is oriented 90° to the plane of the polarized light.

ature was finally confirmed by dynamic time sweep (DTS) measurements at 0.1 % strain and 1 Hz frequency.

Interestingly, a thixotropic response^[26] to the large external strain of the gel made in glycerol was confirmed by a three-step loop test^[27] consisting of the initial application of a shear

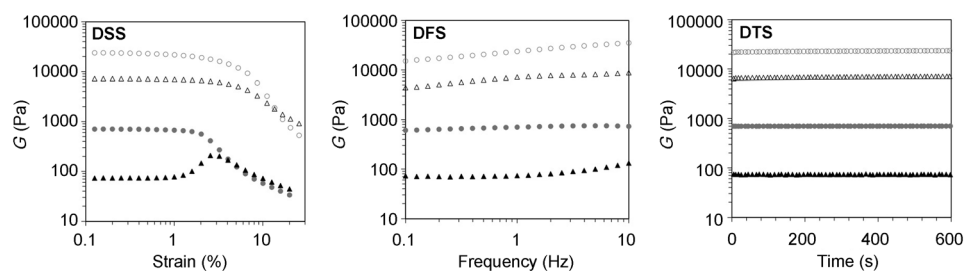


Figure 14. Representative oscillatory rheological experiments (DSS, DFS, DTS) of model gels prepared in toluene and glycerol (90 wt.%) at 5 g L⁻¹. ○: G' (Tol); △: G'' (Tol); ●: G' (Gly); ▲: G'' (Gly).

strain as defined by DTS experiments ($G' > G''$ -gel-), further increase of the strain until the gel fractures ($G' < G''$ -sol-) and final return at the same rate to the initial strain value ($G' > G''$ -gel-). Figure 15 shows up to 50% recovery of the original gel strength within 1 min after the second step and full recovery after 3 h. The thixotropic behavior was also macroscopically observed in a glass vial upon a vigorous shaking/resting cycle. This property is highly pursued for the use of gel-based materials in many real-life applications.

Responsiveness to silver ions

Responsiveness tests of model gels in the presence of various ions revealed that they maintained their integrity after incubation with CuSO₄, NaI, KOAc, or KNO₃ aqueous solutions (0.1 M). However, glycerol gel showed an evident color change from colorless to orange/brownish after 30 min in the presence of solutions containing Ag⁺ ions (e.g., AgNO₃, AgOAc, AgOTf) (Figure 16A). The color change was still visible to the naked eye after 24 h for concentrations of Ag⁺ ions as low as 0.01 mM. A series of control experiments demonstrated that the counterion was not involved in the alteration of the color. In addition, the presence of the urea was necessary for the optical change, albeit it was neither limited to compound 1 nor to the

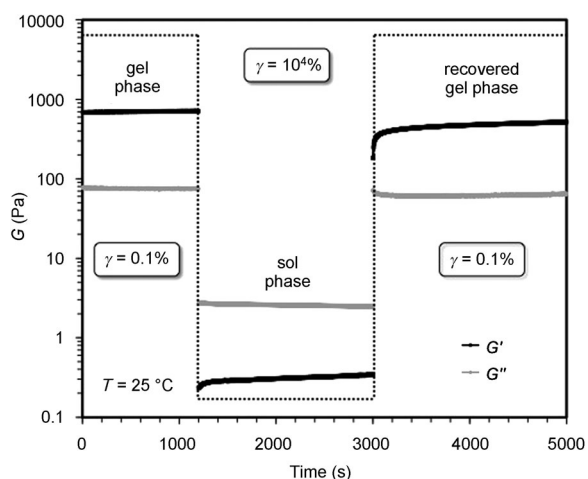


Figure 15. Loop test of the gel made from **1** at CGC in glycerol (90 wt.%). Steps: 1) 1 Hz, 0.1% strain, 20 min ($\tan \delta = 0.1017 \pm 0.002$); 2) 1 Hz, 10000% strain, 30 min; 3) 1 Hz, 0.1% strain ($\tan \delta = 0.108 \pm 0.002$).

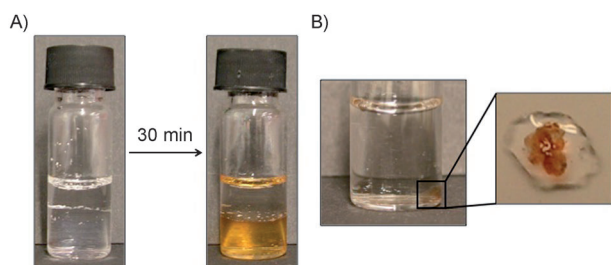


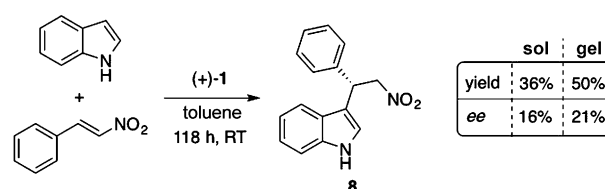
Figure 16. A) Color change of the glycerol-gel phase upon addition of a 0.1 M AgNO_3 solution on top. B) Detection of Ag^+ ions in aqueous solution by using a piece of glycerol gel made of **1** at CGC. Zoom-in: Removal of the piece of gel after coloring.

existence of the gel phase. Thus, the color change was also observed either with compound **1** at a concentration below the CGC or in the presence of other urea analogues in solution, which is in agreement with the considerable tendency of urea compounds to coordinate Ag^+ salts.^[28] Furthermore, the colorimetric test was also compatible with other solvents (e.g. pinkish and yellowish colors were observed in CH_3CN and THF, respectively), albeit glycerol provided the best results in terms of color intensity.

In contrast to a solution of urea **1**, the use of the glycerol gel was more convenient as a colorimetric assay. For instance, a piece of gel could be added to the aqueous solution to be tested for the presence of Ag^+ ions. Afterwards, the gel fragment could be easily separated from the solution by decantation (Figure 16B). UV/Vis spectroscopy of the colored gel showed a broad absorbance peak in the range 400–500 nm (Figure S19A), which has been previously associated with the formation of stable silver nanoparticles by simple glycerol oxidation in the absence of any stabilizer.^[29]

Catalytic alkylation reaction in gel media

During the last decade, a number of publications have shown the potentiality of functional gels as recyclable catalysts and/or



Scheme 2. Alkylation of 1H-indole with *trans*- β -nitrostyrene in solution and the gel phase.

reaction vessels with enhanced selectivity.^[30] Within our research program devoted to investigate reactivities in organized and confined media, we also decided to examine the ability of the self-assembled gel network made from **1** to serve as a nanoreactor for the metal-free Friedel–Crafts alkylation of 1H-indole with *trans*- β -nitrostyrene (Scheme 2). We have previously studied both urea **1** and thiourea **2** as organocatalysts for this reaction in solution.^[9] The results obtained there clearly demonstrated a higher catalytic efficiency for the thiourea, which was attributed to its greater hydrogen-bond donor ability and less tendency to self-assembly in comparison to **1**. Remarkably, when the above reaction was carried out in the gel phase provided by **1** in toluene, the product yield of **8** increased approximately 1.4-fold compared with that in solution (Figure S18, Supporting Information).

This result is especially relevant if we consider that kinetics of diffusion-controlled processes can be 10–20 times faster in stirred solutions than in nonstirred gel media.^[31] In addition, the average level of enantioselectivity observed in the gel phase was slightly superior than in solution, which may suggest among different possibilities that the fibrillar network could somehow provide an additional shielding effect responsible for facial discrimination. In addition, the supramolecular porous network could also contribute to some level of catalyst spatial isolation, which has been elegantly achieved by means of porous MOF environments for which the reaction occurs primarily within the pores.^[32]

Conclusion

The results of this study confirm the potential of some urea-based organocatalysts, such as **1**, as building blocks for the preparation of physical organogels at concentrations ranging from 3 to 50 g L^{-1} . According to FTIR, NMR, and quantum-mechanical studies, the major driving forces for the gelation of organic solvents by **1** are hydrogen-bonding and π - π interactions. In comparison to the Hansen solubility parameters, the Kamlet–Taft solvatochromic parameters offer here a more convenient scenario to rationalize the gelation ability. Moreover, a variety of morphologies including helical, laths, macroporous, or lamellar nanostructures could be obtained depending on the solvent nature. Variations of the most important structural segments (compounds **2**–**7**) that could influence the self-assembly of **1** and computer modeling proved the existence of unique molecular interactions in this molecule that drive the formation of stable hierarchical supramolecular aggregates.

Multistimuli responsive behaviors (e.g., thermal, mechanical, optical, and chemical responses) and a multifunctional nature were demonstrated in some of the gel materials. In this respect, **1** could be used for the phase selective gelation of oil/water mixtures, the gel in glycerol was found to be thixotropic and provided a sensing ability for Ag⁺ ions at millimolar concentrations in aqueous solutions. In addition, the gel matrix obtained in toluene behaved as a nanoreactor for the Friedel–Crafts alkylation of 1*H*-indole with *trans*- β -nitrostyrene catalyzed by **1**. Efforts towards the development of other multifunctional materials are currently underway in our laboratories.

Experimental Section

Synthesis and characterization of compounds

Materials: All commercially available solvents and reagents for synthesis and analysis were used as received without further purification. Compound **4** was available from commercial sources.

Characterization methods: Purification of reaction products was carried out by flash chromatography using silica gel (0.063–0.200 mm) or medium-pressure liquid chromatography by using prepacked silica columns. Analytical TLC analysis was performed on 0.25 mm silica gel 60-F plates. The products were visualized by exposure to UV light (254 nm) and phosphomolybdic acid as a stain. MS were obtained by using ESI ionization on a Bruker Daltonics Esquire 3000 plus (MicroToF-Q) spectrometer. Unless otherwise indicated, NMR spectra were recorded at room temperature on a Bruker AVANCE-II instrument. ¹H NMR spectra were recorded at 400 MHz and ¹³C NMR spectra were recorded at 100 MHz, by using [D₆]DMSO and D₃CCOCD₃ as the deuterated solvents. Chemical shifts were reported in the δ scale relative to residual DMSO (δ = 2.50 ppm for ¹H NMR spectra and δ = 39.43 ppm for ¹³C NMR spectra) and acetone (δ = 2.05 ppm for ¹H NMR spectra). Coupling constants (*J*) were expressed in Hertz. Melting points were determined on a Gallenkamp variable heating apparatus. Optical rotations were measured in a JASCO DIP-370 polarimeter. IR spectra were recorded on a Nicolet Avatar 360 FTIR spectrophotometer. HPLC was carried out by using a Waters 2695 Alliance detector.

General procedure for the synthesis of compounds 1–3 and 5–7: The corresponding commercially available amine (1.0 mmol) (i.e., (1*S*,2*R*)-1-amino-2,3-dihydro-1*H*-inden-2-ol for compounds **1**, **2**, and **7**; (1*R*,2*R*)-1-amino-2,3-dihydro-1*H*-inden-2-ol for compound **5**; 3,5-bis(trifluoromethyl)aniline for compound **3**; (*R*)-2,3-dihydro-1*H*-inden-1-amine for compound **6**) was added in one portion to a stirred solution of 3,5-bis(trifluoromethyl)phenyl isocyanate (1.1 mmol; for the synthesis of compounds **1**, **3**, **5**, and **6**), 3,5-bis(trifluoromethyl)phenyl isothiocyanate (1.1 mmol; for the synthesis of compound **2**), or phenyl isocyanate (1.1 mmol; for the synthesis of compound **7**) in CH₂Cl₂ (5 mL). After stirring the resulting solution at room temperature overnight, the solvent was evaporated under reduced pressure and the product was purified by flash chromatography or medium-pressure liquid chromatography (SiO₂, hexane/EtOAc 7:3). ¹H and ¹³C NMR spectra for compounds (+)-**1**,^[33] (–)-**1**,^[34] **2**,^[9] and **3**^[35] were consistent with values previously reported in the literature.

1-[3,5-Bis(trifluoromethyl)phenyl]-3-[(1*R*,2*R*)-2-hydroxy-2,3-dihydro-1*H*-inden-1-yl]urea (5**):** Following the general procedure, compound **5** was obtained as a white solid in 92% yield. M.p. 232–234 °C; [α]_D²⁰ = –88.1 (*c* = 0.74 in DMSO); ¹H NMR (400 MHz, [D₆]DMSO): δ = 9.21 (brs, 1H), 8.14 (s, 2H), 7.57 (s, 1H), 7.22–7.19

(m, 4H), 6.89 (d, *J* = 8.3 Hz, 1H), 5.33 (d, *J* = 5.5 Hz, 1H), 4.95 (dd, *J* = 6.7, 8.1 Hz, 1H), 4.29–4.22 (m, 1H), 3.14 (dd, *J* = 7.1, 15.6 Hz, 1H), 2.72 ppm (dd, *J* = 7.27, 15.6 Hz, 1H); ¹³C NMR (100 MHz, [D₆]DMSO): δ = 154.9, 142.4, 141.8, 139.6, 130.5 (q, *J* = 32.5 Hz, CCF₃), 127.6, 126.6, 124.6, 123.8, 123.3 (q, *J* = 272.8 Hz, CF₃), 117.5–117.2 (m, 1C), 113.6–113.4 (m, 1C), 77.9, 61.6, 38.5 ppm; IR (KBr film): $\tilde{\nu}$ = 3395, 3326, 2923, 2853, 1634, 1278, 1129, 1073, 749 cm^{–1}; MS (ESI): *m/z*: calcd for C₁₈H₁₄F₆N₂NaO₂: 427.1; found: 427.1 [*M*+Na].

(*R*)-1-[3,5-Bis(trifluoromethyl)phenyl]-3-(2,3-dihydro-1*H*-inden-1-yl)urea (6**):** By following the general procedure, compound **6** was obtained as a white solid in 75% yield. M.p. 215–217 °C; [α]_D²² = –48.7 (*c* = 0.77 in DMSO); ¹H NMR (400 MHz, CD₃COCD₃): δ = 8.58 (brs, 1H), 8.20 (s, 2H), 7.55 (s, 1H), 7.36–7.34 (m, 1H), 7.26–7.17 (m, 3H), 6.34 (brd, *J* = 7.3 Hz, 1H), 5.35 (q, *J* = 7.7 Hz, 1H), 2.96 (ddd, *J* = 3.6, 8.7, 15.9 Hz, 1H), 2.89–2.81 (m, 1H), 2.59–2.51 (m, 1H), 1.91–1.82 ppm (m, 1H); ¹³C NMR (100 MHz, [D₆]DMSO): δ = 154.6, 143.9, 142.7, 142.4, 130.5 (q, *J* = 32.5 Hz, CCF₃), 127.4, 126.3, 124.5, 123.7, 123.3 (q, *J* = 272.8 Hz, CF₃), 117.4–117.3 (m, 1C), 113.6–113.4 (m, 1C), 54.5, 33.3, 29.5 ppm; IR (KBr film): $\tilde{\nu}$ = 2923, 2853, 1639, 1457, 1276, 1130 cm^{–1}; MS (ESI): *m/z*: calcd for C₁₈H₁₄F₆N₂NaO: 411.1; found: 411.1 [*M*+Na].

1-[(1*S*,2*R*)-2-Hydroxy-2,3-dihydro-1*H*-inden-1-yl]-3-phenylurea (7**):** Following the general procedure, compound **7** was obtained as white solid in 94% yield. M.p. 224–226 °C; [α]_D²¹ = +53.9 (*c* = 0.64 in DMSO); ¹H NMR (400 MHz, [D₆]DMSO): δ = 8.85 (s, 1H), 7.45 (d, *J* = 8.5 Hz, 1H), 7.26–7.18 (m, 6H), 6.91 (t, *J* = 7.3 Hz, 1H), 6.44 (d, *J* = 8.7 Hz, 1H), 5.24 (d, *J* = 4.2 Hz, 1H), 5.10 (dd, *J* = 5.0, 8.5 Hz, 1H), 4.45 (dd, *J* = 4.1, 8.9 Hz, 1H), 3.07 (dd, *J* = 4.8, 16.2 Hz, 1H), 2.80 ppm (d, *J* = 16.2 Hz, 1H); ¹³C NMR (100 MHz, [D₆]DMSO): δ = 155.2, 143.1, 140.5, 140.3, 128.6, 127.0, 126.2, 124.8, 123.8, 120.9, 117.4, 72.0, 57.1, 39.6 ppm; IR (KBr film): $\tilde{\nu}$ = 3469, 3365, 3292, 2923, 2854, 1623, 1568, 1458, 1246, 1050, 766, 748, 735 cm^{–1}; MS (ESI): *m/z*: calcd for C₁₆H₁₆N₂NaO₂: 291.1; found: 291.1 [*M*+Na].

Preparation and characterization of gel materials

Characterization methods: Oscillatory rheological measurements were performed at 25 °C with an AR 2000 Advanced Rheometer from TA Instruments equipped with a cooling system (Julabo C). A 20 mm plain plate geometry (stainless steel) was used. Dynamic strain sweep (DSS) measurements were first carried out between 0.01% and 100% strain at 1 Hz frequency to estimate the strain value at which reasonable torque values were given (i.e., about 10 times of the transducer resolution limit). Dynamic frequency sweep (DFS) measurements (i.e., from 0.1 to 10 Hz at 0.1% strain) and time sweep measurements (DTS) within the viscoelastic regime (i.e., 0.1% strain, 1 Hz frequency) were subsequently performed. Additionally, the thixotropic behavior of the gels was investigated by a 3-step loop experiment: 1) Application of a low shear strain as established by previous DTS experiments (the material is in the gel state, *G'* > *G''*), 2) increase of the shear strain until the gel fractures (the material turns into a viscous solution, *G'* < *G''*), and 3) return at the same rate to the initial strain% value (the gel phase has been recovered, *G'* > *G''*). FTIR spectra were recorded by using a Diamond ATH (attenuated total reflection) accessory (Golden Gate) in a VARIAN 1000 FTIR Scimitar™ Series spectrophotometer. Morphological characterization of the samples was carried out by TEM, field-emission SEM (FESEM) and atomic force microscopy (AFM). a) TEM: Images were recorded using a JEOL-2000 FXII TEM (resolution = 0.28 nm) equipped with a CCD Gatan 694 digital camera and operating at 10 kV (accelerating voltage). Sample preparation: 10 μ L of the gel suspension was allowed to adsorb for 30 s onto

carbon-coated grids (300 mesh, from TED PELLA, Inc.). After the adsorption, the excess solvent was removed by touching the edges with a small piece of filter paper. The specimens were then dried overnight in a desiccator at low pressure and RT. b) FESEM: Images were obtained with a Carl Zeiss Merlin field emission SEM (FESEM, resolution = 0.8 nm resolution) equipped with a digital camera and operating at 10 kV (accelerating voltage) and 10 mA (emission current). Sample preparation: Specimens were prepared by the freeze-drying method.^[36] Prior to imaging, a 5 nm sized Pt film was sputtered (40 mA, 30 seconds) on the samples placed on carbon tape. c) AFM: Imaging was performed on a Ntegra Aura (NT-MDT) instrument in tapping mode at 1 Hz scanning rate using directly polycrystalline sapphire (24 × 19.3 × 0.5 mm) as substrate and a single-crystal silicon tip coated with TiN (NSG01/TiN, 0.01–0.025 Ω cm, Antimony doped) at 200–400 kHz drive frequency. Drive amplitude ranged from 60 to 100 mV. Sample preparation: 5–10 μL of a gel suspension (ca. 10-fold dilution in the corresponding solvent) was placed on the substrate and homogeneously dispersed with a spatula to form a thin layer that was allowed to dry in air for at least 30–60 min before measurement. The growth of crystals in gel phases was monitored using a Wild Makroskop M420 optical microscope equipped with a Canon Power shot A640 digital camera for digital imaging. An additional polarization filter was used to observe the gel material under polarized light. Differential scanning calorimetry (DSC) spectra were measured on a DSC7 (PerkinElmer) instrument at a scan rate of 10 °C min⁻¹ under a nitrogen atmosphere. For the measurements, an appropriate amount of gel was placed into a pre-weighted Al pan, which was sealed and weight on a six-decimal plate balance. The pans were weighted again after each measurement to check for possible leakage. Temperature-dependent ¹H NMR spectroscopic studies were carried out on a 400 MHz Bruker Avance instrument equipped with a BVT 2000 heating system (Bruker BioSpin GmbH). Specific surface area, pore volume, pore-size and gas adsorption/desorption isotherms were measured by a Micromeritics ASAP 2020 analyzer at 77 K after vacuum degassing of the sample at 80 °C for 24 h. Powder X-ray diffraction (PXRD) patterns were collected on a Rigaku D/max-2500 rotating-anode powder diffractometer with Cu_{Kα} radiation operated at 40 kV and 80 mA. Conditions: 0.03°, time 5 s/step, 2 theta range 5–60°. Distilled water contact angles and surface energies were measured with a PG goniometer (ASTM D5946) with the droplet size (4 μL) controlled by a pump-dosing unit. Absorption spectra were recorded on a Varian Cary BIO 50 UV/Vis scanning spectrophotometer by using 1 cm quartz cuvettes (Suprasil®, Hellma). Critical gelation concentrations, CGC, were estimated by adding solvent in several portions (0.1 mL each) into the vial where no gelation was achieved at the previous concentration and some material remained insoluble. The initial concentration for gelation tests was 5 g L⁻¹. The state of the mixture was determined after the heating-cooling cycle as described above. New tests were carried out at lower concentration if stable clear solutions were obtained at 5 g L⁻¹. Gel-to-sol transition temperatures, *T*_{gel}, were typically determined by the inverse flow method. The average values of at least two random experiments were given. The seal vial containing the organogel was hung horizontally into an oil bath, which was heated up at 2 °C min⁻¹. Herein, the temperature at which the gel started to break was defined as *T*_{gel}. These values were correlated with the first DSC endothermic transition of selected examples.

General procedure for the preparation of organogels: Solvents used for gelation tests were purchased from commercial suppliers and were at least of p.a. quality. Typically, a weighted amount of the corresponding compound (1–7) and 1 mL of the appropriate

solvent were placed into a screw-capped glass vial (4.5 cm length × 1.2 cm diameter). The closed vial was gently heated with a heat gun until the solid material was completely dissolved. The resulting isotropic solution was then spontaneously cooled down to room temperature. The material was preliminary classified as a gel if it did not exhibit gravitational flow upon turning the vial upside-down at room temperature. The gel state was further confirmed by rheological measurements.

Phase-selective gelation tests: The specified amount of the gelator (+)-1 according to its CGC, the desired organic solvent (1.0 mL), and distilled water (1.0 mL) were added to a screw-capped glass vial (4.5 cm length × 1.2 cm diameter). The vial was closed and gently heated with a heat gun until the gelator was dissolved. The state of the material was evaluated after cooling down the mixture to room temperature by turning the vial upside-down.

Responsiveness experiments: Gel material 1.0 mL was prepared at the corresponding CGC as described above. The gel was allowed to equilibrate for at least 1 h before 1.0 mL of test solution (e.g., 1.0 mL with 0.1 M AgNO₃) was placed on top of the gel. The effect of the test solution on the gel (e.g., induction to gel-to-sol transition, color change) was monitored over time at room temperature.

Friedel-Crafts alkylation in gel media: Dry toluene (0.1 mL) was added to a screw-capped vial containing a mixture of *trans*-β-nitrostyrene (0.1 mmol), 1*H*-indole (0.15 mmol), and 20 mol% of the urea gelator (+)-1. The mixture was gently heated until an isotropic solution was formed. Complete gelation occurred within 20 min and the reaction was allowed to proceed for 118 h at room temperature. After this time, the solvent was removed under reduced pressure. The crude product was analyzed by NMR spectroscopy using DMA (0.1 mol) as the internal standard. For HPLC analysis, the product was purified by column chromatography using *n*-hexanes/ethyl acetate 8:2 as the eluent.

Quantum-mechanical calculations: Quantum-mechanical calculations were performed by using the Gaussian 09^[37] computer program, applying default thresholds and algorithms. The *meta*-generalized gradient approximation (GGA) functional M06L of Truhlar and Zhao^[38] was combined with the 6–31 + G(d,p)^[39] basis set for calculations on dimers of 1–7. The M06L function is known to provide geometry and interaction energy of dimers stabilized by non-covalent interactions, including π-stacking, with accuracy close to that of coupled cluster with both single and double substitutions (CCSD).^[40] Environmental effects (here dichloromethane) have been accounted for using the well-known Polarizable Continuum Model (PCM) model.^[41] Complete geometry optimizations of all dimer were performed by using the PCM approach. Intermolecular interaction energies in the gas phase (i.e., in absence of environmental forces) were estimated as the difference between the energy in the gas-phase of the dimer optimized in dichloromethane solution and the energies of the isolated subsystems in the gas-phase with the geometries obtained from the optimization in solution of the dimer. The basis set superposition error of the energies of the subsystems were corrected using the counterpoise (CP) method.^[42] Similarly, intermolecular interaction energies in dichloromethane were calculated as the difference between the energies in solution of the dimer and the subsystems.

Acknowledgements

Financial support from the Universität Regensburg (Förderlinie C des Finanziellen Anreizsystems für Drittmittelwerbung), Spanish Ministry of Economía y Competitividad (MINECO,

Madrid, Spain, Projects CTQ2010–19606 and MAT2012–34498), and the Governments of Aragón (Zaragoza, Spain, Research Group E-10) and Catalunya (research group 2009 SGR 925, XRQTC and “ICREA Academia” Award for excellence in research to C.A.) is gratefully acknowledged. We thank Prof. A. Göpferich (Universität Regensburg) for granting us access to the AR 2000 rheometer, Prof. P. Cea, Dr. S.M. Solans, and Dr. R. Mallada (Universidad de Zaragoza), Dr. R. Banerjee and P. Pachfule (NCL, Pune, India), for discussions and/or helpful assistance with some measurements. C.A. is indebted to the Centre de Supercomputació de Catalunya (CESCA) for the computational resources provided. D.D.D. thanks the DFG for the Heisenberg Professorship Award.

Keywords: multifunctional materials · multistimuli responsiveness · organogels · self-assembly · ureas

- [1] S. M. Mukhopadhyay, *Nanoscale Multifunctional Materials: Science and Applications*, John Wiley & Sons, Inc., Hoboken, NJ, US, **2011**.
- [2] a) X. Y. Liu, *Top. Curr. Chem.* **2005**, *256*, 1–37; b) M. de Loos, B. L. Feringa, J. H. van Esch, *Eur. J. Org. Chem.* **2005**, 3615–3631; c) *Molecular Gels: Materials with Self-Assembled Fibrillar Networks* (Eds.: R. G. Weiss, P. Terech), Springer, Netherlands, 2006, pp. 449–551; d) M. George, R. G. Weiss, *Acc. Chem. Res.* **2006**, *39*, 489–497; e) G. C. Maity, *J. Phys. Sci.* **2007**, *11*, 156–171; f) E. Zaccarelli, *J. Phys. Condens. Matter* **2007**, *19*, 323101; g) S. Banerjee, R. K. Das, U. Maitra, *J. Mater. Chem.* **2009**, *19*, 6649–6687.
- [3] a) D. Derossi, Y. Kajiwar, Y. Osada, *Polymer Gels: Fundamentals and Bio-medical Applications*, Plenum Press, New York, **1991**, and references therein; b) J. H. Jung, S. Shinkai, *Top. Curr. Chem.* **2005**, *248*, 223–260; c) N. M. Sangeetha, U. Maitra, *Chem. Soc. Rev.* **2005**, *34*, 821–836; d) R. V. Uljin, A. M. Smith, *Chem. Soc. Rev.* **2008**, *37*, 664–675; e) M. O. M. Piepenbrock, G. O. Lloyd, N. Clarke, J. W. Steed, *Chem. Rev.* **2010**, *110*, 1960–2004.
- [4] a) T. Tanaka, *Sci. Am.* **1981**, *244*, 124; b) Y. Osada, A. R. Khokhlov, *Polymer Gels and Networks*; Marcel Dekker: New York, 2002; c) S.-k. Ahn, R. M. Kasi, S.-C. Kim, N. Sharma, Y. Zhou, *Soft Matter* **2008**, *4*, 1151–1157.
- [5] a) L. A. Estroff, A. D. Hamilton, *Chem. Rev.* **2004**, *104*, 1201–1218, and references therein; b) P. Xie, R. Zhang, *J. Mater. Chem.* **2005**, *15*, 2529–2550; c) D. K. Smith, *Chem. Commun.* **2006**, 34–44; d) D. J. Adams, *Macromol. Biosci.* **2011**, *11*, 160–173; e) A. Dawn, T. Shiraki, S. Haraguchi, S. Tamaru, S. Shinkai, *Chem. Asian J.* **2011**, *6*, 266–282; f) X. Yang, G. Zhang, D. Zhang, *J. Mater. Chem.* **2012**, *22*, 38–50.
- [6] A. Ajayaghosh, V. K. Praveen, C. Vijayakumar, *Chem. Soc. Rev.* **2008**, *37*, 109–122.
- [7] a) S. K. Chandran, N. K. Nath, S. Cherukuvada, A. Nangia, *J. Mol. Struct.* **2010**, *968*, 99–107; b) R. Custelcean, *Chem. Commun.* **2008**, 295–307; c) J. Rebeck Jr., *Chem. Commun.* **2000**, 637–643; d) A. Bogdan, V. Rudzevich, M. O. Vysotsky, V. Böhmer, *Chem. Commun.* **2006**, 2941–2952.
- [8] M. Yamanaka, *J. Inclusion Phenom. Macrocyclic Chem.* **2013**, *77*, 33–48, and references therein.
- [9] a) R. P. Herrera, V. Sgarzani, L. Bernardi, A. Ricci, *Angew. Chem.* **2005**, *117*, 6734–6737; *Angew. Chem. Int. Ed.* **2005**, *44*, 6576–6579; b) G. Dessole, R. P. Herrera, A. Ricci, *Synlett* **2004**, 2374–2378.
- [10] See the Supporting Information for further details.
- [11] X. Fan, R. Burton, *Open Fuel Energy Sci. J.* **2009**, *2*, 100–109.
- [12] A. Takahashi, M. Sakai, T. Kato, *Polym. J.* **1980**, *12*, 335–341.
- [13] I. Kapoor, E.-M. Schön, J. Bachl, D. Kühbeck, C. Catiavela, S. Saha, R. Banerjee, S. Roelens, J. J. Marrero-Tellado, D. D. Diaz, *Soft Matter* **2012**, *8*, 3446–3456.
- [14] a) Z. Dzolic, K. Wolsperger, M. Žinić, *New J. Chem.* **2006**, *30*, 1411–1419; b) A. Bizard, R. Oda, I. Huc, *Top. Curr. Chem.* **2005**, *256*, 167–218.
- [15] a) S. R. Jadhav, P. K. Vemula, R. Kumar, S. R. Raghavan, G. John, *Angew. Chem.* **2010**, *122*, 7861–7864; *Angew. Chem. Int. Ed.* **2010**, *49*, 7695–7698; b) S. Bhattacharya, Y. Krishnan-Ghosh, *Chem. Commun.* **2001**, 185–186.
- [16] a) A. Prathap, K. M. Sureshan, *Chem. Commun.* **2012**, *48*, 5250–5252; b) S. Basak, J. Nanda, A. Banerjee, *J. Mater. Chem.* **2012**, *22*, 11658–11664; c) S. Debnath, A. Shome, S. Dutta, P. K. Das, *Chem. Eur. J.* **2008**, *14*, 6870–6881.
- [17] X. Yu, Y. Li, D. Wu, Z. Ma, S. Xing, *New J. Chem.* **2013**, *37*, 1201–1205.
- [18] M. J. Kamlet, J. L. M. Abboud, M. H. Abraham, R. W. Taft, *J. Org. Chem.* **1983**, *48*, 2877–2887.
- [19] M. Raynal, L. Bouteiller, *Chem. Commun.* **2011**, *47*, 8271–8273.
- [20] A. R. Hirst, D. K. Smith, *Langmuir* **2004**, *20*, 10851–10857.
- [21] P. Fatás, J. Bachl, S. Oehm, A. I. Jiménez, C. Catiavela, D. D. Diaz, *Chem. Eur. J.* **2013**, *19*, 8861–8874.
- [22] a) F. Allix, P. Curcio, Q. N. Pham, G. Pickaert, B. Jamart-Grégoire, *Langmuir* **2010**, *26*, 16818–16827; b) J. Makarevic, M. Jokic, Z. Raza, Z. Stefanic, B. Kojic-Prodic, M. Zinic, *Chem. Eur. J.* **2003**, *9*, 5567–5580.
- [23] a) L. Frkanec, M. Zinic, *Chem. Commun.* **2010**, *46*, 522–537; b) V. Caplar, M. Zinic, J.-L. Pozzo, F. Fages, G. Mieden-Gundert, F. Vögtle, *Eur. J. Org. Chem.* **2004**, 4048–4059.
- [24] a) R. M. Osuna, V. Hernández, J. T. L. Navarrete, E. D’Oria, J. J. Novoa, *Theor. Chem. Acc.* **2011**, *128*, 541–553; b) K. E. Riley, P. Hobza, *J. Chem. Theory Comput.* **2008**, *4*, 232–242.
- [25] R. E. Fischer, B. Tadic-Galeb, P. R. Yoder, *Optical System Design*, McGraw Hill, 2nd Ed., **2008**.
- [26] a) P. Kirilov, F. Gauffre, S. Franceschi-Messant, E. Perez, I. Rico-Lattes, *J. Phys. Chem. B* **2009**, *113*, 11101–11108; b) T. Peterfi, *Arch. Entwicklungsmech. Organ.* **1927**, *112*, 680–686.
- [27] a) G. Mezger, *The Rheology Handbook*, Vincentz Network, Hannover, Germany, 2011; b) H. A. Barnes, *J. Non-Newtonian Fluid Mech.* **1997**, *70*, 1–33.
- [28] a) M. Salman, *Int. J. Life Sci. Pharm. Res.* **2012**, *2*, 128–138; b) M.-O. M. Piepenbrock, N. Clarke, J. W. Steed, *Soft Matter* **2011**, *7*, 2412–2418.
- [29] K. Patel, S. Kapoor, D. P. David, T. Mukherjee, *J. Chem. Sci.* **2005**, *117*, 53–60.
- [30] D. D. Diaz, D. Kuhbeck, R. J. Koopmans, *Chem. Soc. Rev.* **2011**, *40*, 427–448.
- [31] J. Bachl, A. Hohenleutner, B. B. Dhar, C. Catiavela, U. Maitra, B. König, D. D. Diaz, *J. Mater. Chem. A* **2013**, *1*, 4577–4588.
- [32] J. M. Roberts, B. M. Fini, A. A. Sarjeant, O. K. Farha, J. T. Hupp, K. A. Scheidt, *J. Am. Chem. Soc.* **2012**, *134*, 3334–3337.
- [33] R. P. Herrera, D. Monge, E. Martín-Zamora, R. Fernández, J. M. Lassaletta, *Org. Lett.* **2007**, *9*, 3303–3306.
- [34] M. P. Sibi, K. Itoh, *J. Am. Chem. Soc.* **2007**, *129*, 8064–8065.
- [35] B. Procuranti, S. J. Connon, *Chem. Commun.* **2007**, 1421–1423.
- [36] S. W. Jeong, S. Shinkai, *Nanotechnology* **1997**, *8*, 179–183.
- [37] a) K. E. Riley, M. Pitoňák, P. Jurečka, P. Hobza, M. J. Frisch, G. W. Trucks, H. B. Schlegel, G. E. Scuseria, M. A. Robb, J. R. Cheeseman, G. Scalmani, V. Barone, B. Mennucci, G. A. Petersson, H. Nakatsuji, M. Caricato, X. Li, H. P. Hratchian, A. F. Izmaylov, J. Bloino, G. Zheng, J. L. Sonnenberg, M. Hada, M. Ehara, K. Toyota, R. Fukuda, J. Hasegawa, M. Ishida, T. Nakajima, Y. Honda, O. Kitao, H. Nakai, T. Vreven, J. A. Montgomery, Jr., J. E. Peralta, F. Ogliaro, M. Bearpark, J. J. Heyd, E. Brothers, K. N. Kudin, V. N. Staroverov, T. Keith, R. Kobayashi, J. Normand, K. Raghavachari, A. Rendell, J. C. Burant, S. S. Iyengar, J. Tomasi, M. Cossi, N. Rega, J. M. Millam, M. Klene, J. E. Knox, J. B. Cross, V. Bakken, C. Adamo, J. Jaramillo, R. Gomperts, R. E. Stratmann, O. Yazyev, A. J. Austin, R. Cammi, C. Pomelli, J. W. Ochterski, R. L. Martin, K. Morokuma, V. G. Zakrzewski, G. A. Voth, P. Salvador, J. J. Dannenberg, S. Dapprich, A. D. Daniels, O. Farkas, J. B. Foresman, J. V. Ortiz, J. Cioslowski, and D. J. Fox, Gaussian 09, Revision C.01, Gaussian, Inc., Wallingford CT, **2010**.
- [38] Y. Zhao, D. G. Truhlar, *J. Chem. Phys.* **2006**, *125*, 194101.
- [39] A. D. McLean, G. S. Chandler, *J. Chem. Phys.* **1980**, *72*, 5639–5648.
- [40] K. Remya, C. H. Suresh, *J. Comput. Chem.* **2013**, *34*, 1341–1353.
- [41] J. Tomasi, B. Mennucci, R. Cammi, *Chem. Rev.* **2005**, *105*, 2999–3094.
- [42] S. F. Boys, F. Bernardi, *Mol. Phys.* **1970**, *19*, 553–566.

Received: March 1, 2014

Published online on June 25, 2014